J. Korean Inst. Electr. Electron. Mater. Eng.
Vol. 35, No. 3, pp. 292-296 May 2022
DOI: https://doi.org/10.4313/JKEM.2022.35.3.12
ISSN 1226-7945(Print), 2288-3258(Online)

Regular Paper

Structural and Electrical Properties of (La,Nd,Sr)MnO_3 Ceramics for NTC Thermistor Devices

Kyeong-Ha Shin[1], Byeong-Jun Park[1], Jeong-Eun Lim[1], Sam-Haeng Lee[1,2], Myung-Gyu Lee[1,2], Joo-Seok Park[2], and Sung-Gap Lee[1]

[1] Department of Materials Engineering and Convergence Technology, Research Institute for Green Convergence Technology (RIGET), Gyeongsang National University, Jinju 52828, Korea
[2] Business Support Division, Korea Institute of Ceramic Engineering and Technology, Jinju 52851, Korea

(Received February 18, 2022; Revised March 2, 2022; Accepted March 7, 2022)

Abstract: $(La_{0.5}Nd_{0.2}Sr_{0.3})MnO_3$ specimens were prepared by a solid-state reaction. In all specimens, X-ray diffraction patterns of an orthorhombic structure were shown. The fracture surfaces of $(La_{0.5}Nd_{0.2}Sr_{0.3})MnO_3$ specimens showed a transgranular fracture pattern be possibly due to La ions (0.122 nm) as a perovskite A-site dopant substituting for Nd ions (0.115 nm) having a small ionic radius. The full-width at half maximum (FWHM) of the Mn 2p XPS spectra showed a value greater than that [8] of the single valence state, which is believed to be due to the overlapping of Mn^{2+}, Mn^{3+}, and Mn^{4+} ions. The dependence of Mn 2p spectra on the Mn^{3+}/Mn^{4+} ratio according to sintering time was not observed. Electrical resistivity resulted in the minimum value of 100.7 Ω-cm for the specimen sintered for 9 hours. All specimens show a typical negative temperature coefficient of resistance (NTCR) characteristics. In the 9-hour sintered specimen, TCR, activation energy, and B25/65-value were -1.24%/℃, 0.19 eV, and 2,445 K, respectively.

Keywords: (La,Nd,Sr)MnO_3, Thermistor, Hopping conduction, Structural properties, Electrical properties

1. INTRODUCTION

Perovskite $R_{1-x}A_xMnO_3$ ceramics exhibit high electrical conductivity and colossal magnetoresistance due to their half-metallic nature. Many studies have been conducted on $R_{1-x}A_xMnO_3$ for advanced magnetic sensors, nonvolatile magnetic random access memories (MRAMs), and information recording devices [1-3]. The electric and magnetic properties of $R_{1-x}A_xMnO_3$ significantly change depending on impurity addition and manufacturing processes. In particular, the paramagnetic-ferromagnetic transition temperature (Curie temperature) and electrical resistance of the manganite material significantly change by substituting trivalent rare-earth elements, such as La, Nd, or Pr, on the R-site or divalent dopants, such as Ca, Sr, Ba, or Pb, on the A-site. In addition, the ferromagnetic metallic behavior generated by substituting divalent ions with perovskite $LaMnO_3$ may be described as a double-exchange mechanism due to the distribution of the mixed valance (Mn^{3+} and Mn^{4+}) of manganese to compensate for the non-uniformity of charges [4,5]. (La,Sr)MnO_3 (LSMO) and (La,Ca)MnO_3 (LCMO) have attracted great interest for their applications as oxide electrode materials and interconnector materials for solid-oxide fuel cells (SOFCs) due to their high electrical conductivity at around room temperature. In this research, high electrical conductivity $(La_{0.5}Nd_{0.2}Sr_{0.3})MnO_3$

✉ **Sung-Gap Lee; lsgap@gnu.ac.kr**

(LNSMO) specimens in which Nd_2O_3 was added to the (La,Sr)MnO_3 materials were manufactured using solid state synthesis, and their structural and electrical properties were measured according to sintering time to confirm their possible application as thermistor devices.

2. EXPERIMENTAL

$(La_{0.5}Nd_{0.2}Sr_{0.3})MnO_3$ specimens were fabricated by solid state synthesis. The raw materials were La_2O_3 (Aldrich, 99.99%), Nd_2O_3 (Adrich, 99.99%), $SrCO_3$ (Adrich, 99.99%), and Mn_2O_3 (Alfa Aesar, 99%). After weighing each raw materials according to the composition formula, ethyl alcohol was used as a dispersion medium, and the materials were mixed and pulverized with a ball mill for 24 hours using zirconia balls. The mixed powders were calcined at 850℃ for 2 hours, and sintered at 1,300℃ for 3 to 12 hours in air. The heating rate was 5℃/min. X-ray diffraction analysis (XRD, D8, Bruker), field-emission scanning electron microscopy (FE-SEM, XL30S, Philips), and X-ray photoelectron spectra (XPS, VG Scientific ESCALAB 250) were used to analyze the structural properties of the specimens. The electrical properties were measured using an LCR meter (PM-6036, Fluke) and an electrometer (Keithley 6517A).

3. RESULTS AND DISCUSSIONS

Figure 1 shows the X-ray diffraction patterns according to the sintering time of the LNSMO specimens, and it shows that all specimens had a polycrystalline XRD shape with an orthorhombic structure. As the sintering time increased, the main peak around $2\theta=32^\circ$ tended to increase, which is thought to be due to the improvement of crystallinity as the grain size increased. A small peak of Mn_3O_4 phase was observed near $2\theta=30^\circ$. According to the La_2O_3-Mn_2O_3 binary phase diagram, Mn_2O_3 transformed to Mn_3O_4 at 1,160℃ in air [6]. In this study, it is believed that some of the transformed Mn_3O_4 was observed as an unreacted substance.

Figure 2 shows the fracture surface of the LNSMO specimens according to the sintering time. The granule-shaped grains and pores were distributed in the LNSMO specimens, and the grain size and pore size increased as the sintering time increased. The fracture surface of the LNSMO specimens showed a transgranular fracture pattern. This is thought to be due to the La ions (0.122 nm) of the perovskite A-site being substituted with Nd ions (0.115 nm), which have a small ionic radius and act as a compressive stress inside the grains and as a tensile stress in the pores by having a large thermal expansion coefficient [7].

Figure 3 shows the XPS analysis of Mn 2p orbital binding energy and the area of the LNSMO specimens according to the sintering time. The Mn 2p XPS spectra showed greater values than FWHM [8] in the single valence state, which is believed to be due to the overlapping of Mn^{2+}, Mn^{3+}, and Mn^{4+} ions. The Mn^{2+}, Mn^{3+}, and Mn^{4+} ion peaks correspond with binding energies of 640.4 to 640.8 eV, 641.6 to 642.1 eV, and 643.0 to

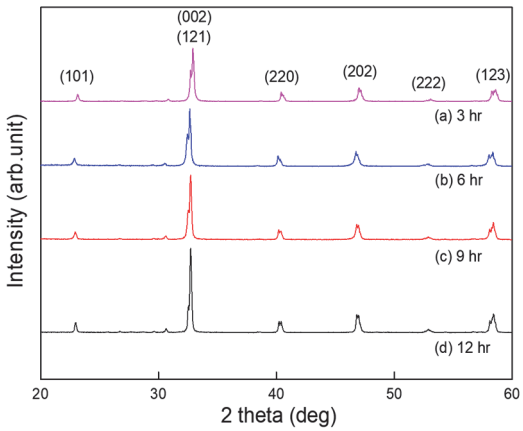

Fig. 1. X-ray diffraction patterns according to the sintering time of LNSMO specimens.

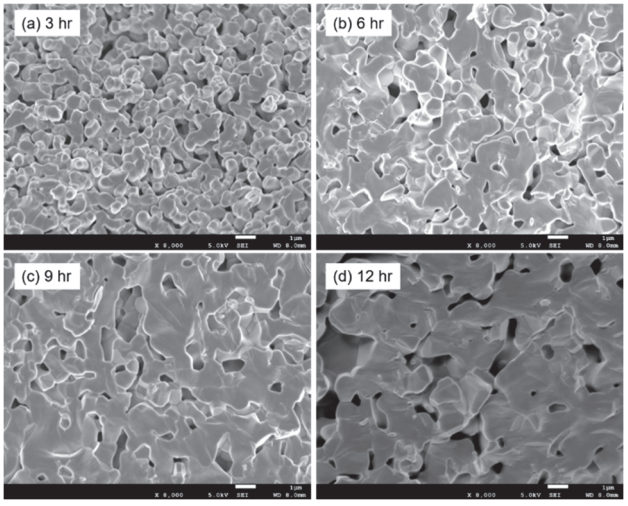

Fig. 2. Fracture surfaces of LNSMO specimens according to the sintering time.

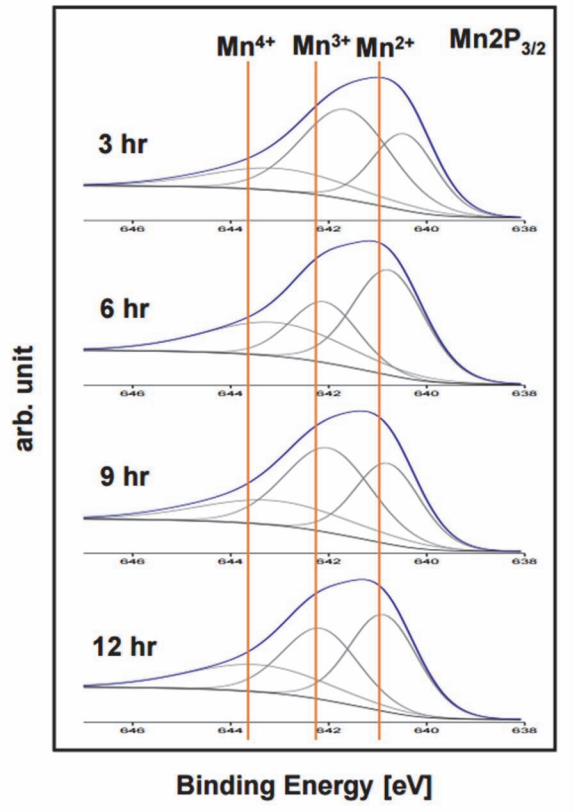

Fig. 3. XPS analysis of the Mn 2p orbital binding energies and area of LNSMO specimens.

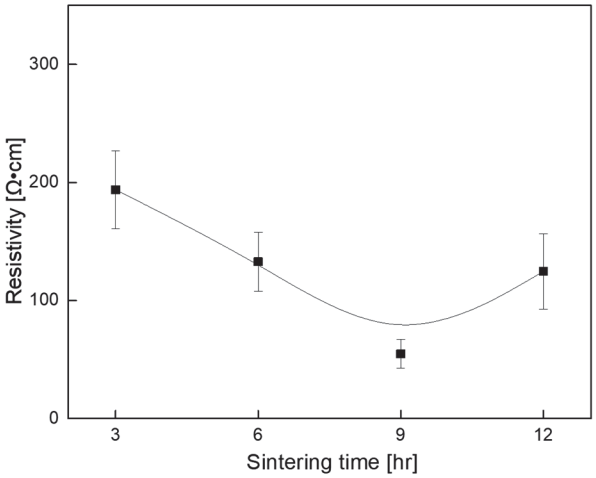

Fig. 4. Resistivity of LNSMO specimens according to the sintering time.

643.4 eV, respectively. The shape of the Mn 2p signal implies that the majority of the Mn ions are mainly in the Mn^{2+} and Mn^{3+} states. Dependence of the Mn 2p spectra on the Mn^{3+}/Mn^{4+} ratio according to the sintering time was not observed.

Figure 4 shows the resistivity of the LNSMO specimens at room temperature according to the sintering time. As the sintering time increased, the resistivity decreased, showing a minimum value of 100.7 Ω-cm in the specimens sintered for 9 hours, and then increasing in the specimens sintered for 12 hours. It is thought that as the sintering temperature increases, the volume ratio of the relatively high resistance grain boundary layers decreases because the grain size of the crystalline structure increases, as shown in Fig. 2. Also, the specimen sintered for 12 hours exhibited high resistivity due to an increase in pores. In general, the electrical conduction of perovskite manganite-based materials occurs by an electron hopping mechanism between the Mn^{3+} and Mn^{4+} ions via oxygen ions [9]. However, in the LNSMO specimens of this study, it is judged that electrical conduction was predominantly affected by structural properties, such as grains, grain boundaries, and pore distribution, rather than hopping conductivity generated in the lattice structure.

Figure 5 shows the electrical resistances according to the sintering time and temperature of the LNSMO specimens. All specimens showed typical negative temperature coefficients of resistance (NTCR). The TCR increased as the sintering time increased, and after showing a maximum of -1.24%/℃ in the specimen sintered for 9 hours, it decreased in the specimen sintered for 12 hours. As shown in Figs. 2 and 4, it is determined that the specimen sintered for 9 hours had the highest TCR because of its relatively good structural properties and high electrical conductivity.

Figure 6 shows the ln(R) vs. 1/T curves of the LNSMO specimens, which have thermally activated behaviors similar to those of semiconductor materials. In colossal magnetoresistance materials, such as LSMO and LCMO, resistive behavior with variation of temperature is expressed as follows: $R(T)=R(0)\exp(Ea/kT)$ [Ω] [10,11], where Ea is the activation energy and k is the Boltzmann constant. Ea can be calculated from the slope in Fig. 6. The LNSMO specimen sintered for 9 hours showed the lowest activation energy of 0.19 eV. The transport exhibited an activated behavior at around room temperature. Generally, electrical conduction in polycrystalline materials is affected by intragrain and intergrain transport based on microscopic structural and chemical characteristics [12].

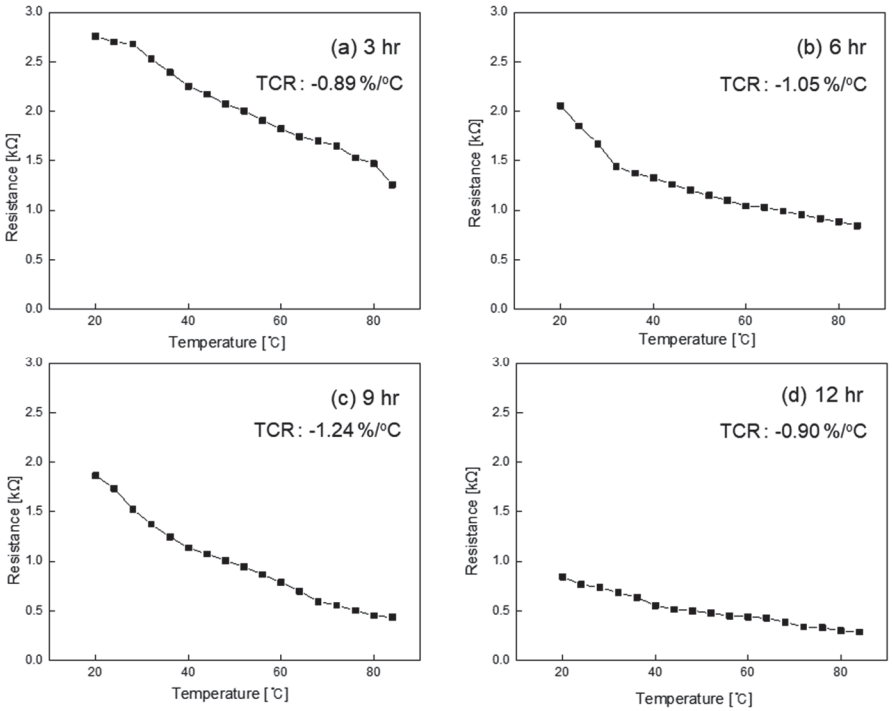

Fig. 5. Electrical resistances of LNSMO specimens according to the sintering time and temperature.

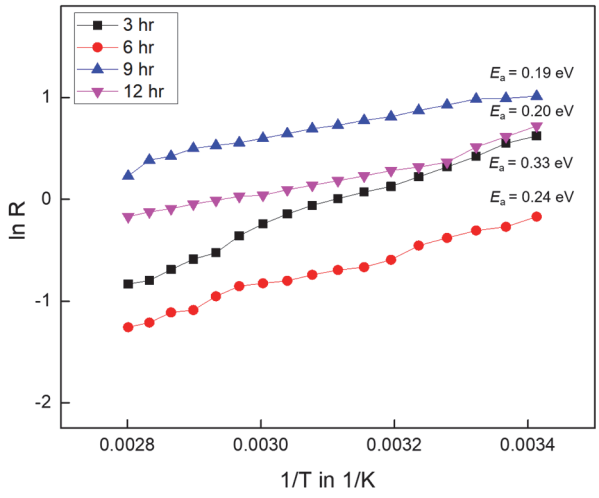

Fig. 6. ln(R) vs. 1/T curves of LNSMO specimens.

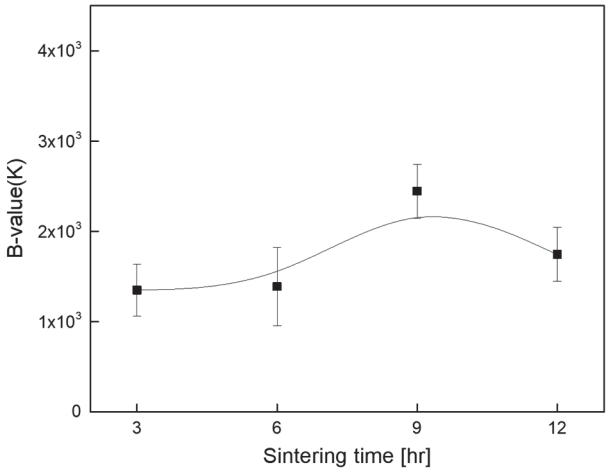

Fig. 7. $B_{25/65}$-value of LNSMO specimens according to the sintering time.

Figure 7 shows the B25/65-value of the LNSMO specimens according to the sintering time. When applied as thermistor devices, the B-value represents a resistance change sensitivity against temperature change. The B25/65-values were calculated from the following equation [13]: B25/65=(lnρ1-lnρ2)/(1/T1-1/T2), where, ρ1 and ρ2 are resistances measured at T1 (25℃) and T2 (65℃), respectively. The B25/65-value increased as the sintering time increased, and after showing a maximum value of 2445K in the specimen sintered for 9 hours, it decreased in the specimen sintered for 12 hours. This is thought to be due to the relative increase in crystalline grain size in the specimen sintered for 9 hours.

4. CONCLUSIONS

In this research, $(La_{0.5}Nd_{0.2}Sr_{0.3})MnO_3$ specimens were fabricated using solid state synthesis, and the structural and electrical properties according to the sintering temperature were measured to observe their applicability as thermistor devices. The microstructures of all specimens were distributed with granule-shaped grains and pores, and the fracture surface showed a transgranular fraction pattern. Generally, the electrical conduction in polycrystalline materials is affected by intragrain and intergrain transport based on microscopic structural and chemical characteristics. It is thought that the electrical conduction properties according to the change of sintering time were predominantly affected by structural properties such as crystal grains, grain boundaries, and pore distribution. The TCR and B25/65-values of the specimen sintered at 1,300℃ for 9 hours were 1.24%/℃ and 2,245 K, respectively, and it is considered that its application as an NTC thermistor device will be possible.

ORCID

Sung-Gap Lee https://orcid.org/0000-0002-3216-0311

ACKNOWLEDGEMENTS

This research was supported by Basic Science Research Program through the National Research Foundation of Korea (NRF) funded by the Ministry of Education (2020R1A6A 1A03038697) and This work was supported by the National Research Foundation of Korea (NRF) grant funded by the Korea government (MSIT) (2021R1I1A3052426).

REFERENCES

[1] Y. Tokura, *J. Appl. Phys.*, **79**, 5288 (1996). [DOI: https://doi.org/10.1063/1.361353]

[2] M. P. de Jong, I. Bergenti, V. A. Dediu, M. Fahlman, M. Marsi, and C. Taliani, *Phys. Rev. B*, **71**, 014434 (2005). [DOI: https://doi.org/10.1103/PhysRevB.71.014434]

[3] K. Tanaka, S. Okamura, and T. Shiosaki, *Jpn. J. Appl. Phys.*, **40**, 6821 (2001). [DOI: https://doi.org/10.1143/JJAP.40.6821]

[4] C. Zener, *Phys. Rev.*, **82**, 403 (1951). [DOI: https://doi.org/10.1103/PhysRev.82.403]

[5] A. Elghoul, A. Krichene, N. C. Boudjada, and W. Boujelben, *Ceram. Int.*, **44**, 12723 (2018). [DOI: https://doi.org/10.1016/j.ceramint.2018.04.075]

[6] J.A.M. van Roosmalen, P. van Vlaanderen, E.H.P. Cordfunke, W. L. Ijdo, and D.J.W. Ijdo, *J. Solid State Chem.*, **114**, 516 (1995). [DOI: https://doi.org/10.1006/jssc.1995.1078]

[7] M. M. Shokrieh, *Residual Stresses in Composite Materials* (Woodhead Publishing, Oxford, 2014) p. 256.

[8] H. W. Nesbitt and D. Banerjee, *Am. Mineral.*, **83**, 305 (1998). [DOI: https://doi.org/10.2138/am-1998-3-414]

[9] K. M. Kim, S. G. Lee, and M. S. Kwon, *Trans. Electr. Electron. Mater.*, **18**, 330 (2017). [DOI: https://doi.org/10.4313/TEEM.2017.18.6.330]

[10] J. Inoue and S. Maekawa, *Phys. Rev. B*, **53**, R11927 (1996). [DOI: https://doi.org/10.1103/PhysRevB.53.R11927]

[11] S. Sahoo, *Trans. Electr. Electron. Mater.*, **21**, 482 (2020). [DOI: https://doi.org/10.1007/s42341-020-00214-y]

[12] M. Uehara, S. Mori, C. H. Chen, and S. W. Cheng, *Nature*, **399**, 560 (1999). [DOI: https://doi.org/10.1038/21142]

[13] E. D. Macklen, *Thermistors* (Electrochemical Publications Ltd. Scotland, 1979) p. 33.